MICROBIOLOGY

MSB2-activated pheromone pathway regulates fungal plasma membrane integrity in response to herbicide adjuvant

Jianwei Pu[1]†, Xiuju Long[1]†, Yifan Li[1]†, Jian Zhang[1], Fei Qi[2], Jiangtao Gao[3], Qirong Shen[1], Zhenzhong Yu[1]*

Glyphosate-based herbicides (GBHs) are used worldwide for weed management. However, GBHs pose a threat to soil fungal community, although fungi can degrade and use glyphosate as a nutrient source. How fungi respond to GBHs remains enigmatic. Here, we found that, not as in plants, the commercial GBH Roundup does not target the 5-enolpyruvyl-shikimate-3-phosphate synthase in the soil-derived fungus *Trichoderma guizhouense*, whereas it impairs fungal growth. We demonstrate that the herbicide adjuvant Triton CG-110 is more toxic to fungal cells than pure glyphosate. It limits nitrogen uptake, which induces the expression of proteinase YPS1 to catalyze the shedding of the MSB2 extracellular domain from the plasma membrane, leading to the activation of the MAPK TMK1 pheromone pathway. The downstream B2H2-type transcription factor STE12 directly regulates ergosterol biosynthesis, affecting membrane fluidity and stability. To our knowledge, this is the first evidence that the pheromone pathway is implicated in ergosterol biosynthesis and plasma membrane integrity.

INTRODUCTION

Glyphosate-based herbicides (GBHs), formulated with glyphosate and formulants, are the most frequently used herbicides for weed management worldwide (*1*). Glyphosate, as the active constituent of GBHs, kills plants mainly by targeting the 5-enolpyruvyl-shikimate-3-phosphate synthase (EPSPS) of the shikimate pathway to block the biosynthesis of aromatic amino acids (*2*). However, the massive use of GBHs in agriculture poses a potential threat to soil microorganisms. Recent studies have shown that GBH application negatively affects soil fungal communities, although fungi can degrade glyphosate (*3*, *4*). Notably, the commercial GBHs appear to exert more detrimental side effects on fungi than the pure glyphosate (*5*, *6*). The mechanisms underlying the side effects of GBHs on fungi remain enigmatic.

Fungi have evolved multiple mitogen-activated protein (MAP) kinase signaling pathways to sense and respond to external signals (*7*, *8*). The pheromone pathway, as the most well-studied one, is implicated in various biological processes, such as asexual and sexual development, cell fusion, secondary metabolism, and virulence (*9*–*13*). The core module of this pathway generally consists of three kinases—MAPKKK, MAPKK, and MAPK—and scaffold and adaptor proteins. The upstream receptors that activate the core module involve the G protein–coupled receptors (GPCRs), which constitute the largest family of the cell surface receptors in eukaryotes, and other receptors such as signaling mucin and plasma membrane-spanning protein for surface signal sensing (*14*–*17*). Activation of the pheromone pathway leads to the phosphorylation of MAPK that subsequently interacts with the transcriptional regulators to regulate gene expression, eliciting a characteristic response to a specific stimulus (*12*).

The integrity of the plasma membrane is integral to the environmental signal sensing of cells, as membrane-bound receptors detect external stimuli and trigger intracellular signaling cascades. Sterols are the basal components of the plasma membrane, crucial for membrane fluidity, permeability, and stability (*18*). Ergosterol, absent in animals and plants, is the major sterol of the fungal plasma membrane, and its biosynthesis relies on a long multistep route involving approximately 20 enzymes in fungi (*19*). *Trichoderma* species as effective biocontrol agents and plant growth stimulators are widely used in agriculture (*20*, *21*). In this study, we investigate the effects of the commercial GBH Roundup (R450) on *Trichoderma* species and reveal how the GBH adjuvant Triton CG-110 induces the shedding of a signaling mucin MSB2 (multicopy suppressor of a budding defect) from the cell surface to activate the pheromone pathway and thus changes the integrity of the plasma membrane by regulating ergosterol biosynthesis.

RESULTS

R450 inhibits fungal hyphal growth and conidial germination

In recent years, more and more beneficial microorganisms have been identified and applied in agriculture, which are inevitably exposed to GBHs (*6*, *22*). *Trichoderma* species are known for their excellent biocontrol and plant growth-promoting roles, in which *Trichoderma guizhouenese*, *Trichoderma harzianum*, and *Trichoderma atroviride* are frequently studied for their interactions with plants and pathogens and applied in agriculture as biocontrol agents and plant growth stimulants (*21*). To investigate the effect of GBHs on the growth of *Trichoderma* species, *T. guizhouenese*, *T. harzianum*, and *T. atroviride* were exposed to different concentrations (0.075 to

[1]Jiangsu Provincial Key Lab for Solid Organic Waste Utilization, Key Lab of Organic-based Fertilizers of China, Jiangsu Collaborative Innovation Center for Solid Organic Wastes, Educational Ministry Engineering Center of Resource-saving fertilizers, Jiangsu Provincial Center for Agricultural Microbial Resource Protection and Germplasm Innovation and Utilization, Nanjing Agricultural University, Nanjing 210095, China. [2]State Key Laboratory of Cellular Stress Biology, School of Life Sciences, Xiamen University, Xiamen 361102, China. [3]State Key Laboratory of Ecological Pest Control for Fujian and Taiwan Crops, College of Life Sciences, Key Laboratory of Biopesticide and Chemical Biology of Ministry of Education, College of Life Sciences, Fujian Agriculture and Forestry University, Fuzhou 350002, China.
*Corresponding author. Email: yuzhenzhong@njau.edu.cn
†These authors contributed equally to this work.

0.225%) of R450, which are all far below the recommended field application rate (2%). We found that the vegetative growth of all the strains tested was inhibited, and the colony edge images showed that the mycelium of *T. guizhouense* was fractured and lysed (Fig. 1, A and B). We further stained the plasma membrane and cell wall with FM 4-64 and Calcofluor White (CFW), respectively, and found that the fluorescence signals for the plasma membrane were increased notably upon R450 treatment (Fig. 1, C and D). Moreover, conidial germination was notably inhibited by R450 (Fig. 1, E and F). These results indicate the negative effects of R450 on hyphal growth and conidial germination.

EPSPS in *T. guizhouense* is not the target of GBH

EPSPS enzymes are categorized into two major classes based on the presence of two specific amino acid markers, glycine-101 and alanine-122, that interact with glyphosate (*23*). Class I enzymes have these crucial amino acid residues and thus are putatively sensitive to glyphosate, whereas class II enzymes are putatively resistant to glyphosate because of the absence of these amino acids. To predict whether the EPSPS enzymes of *Trichoderma* species are sensitive to glyphosate, a phylogenetic analysis was performed on the basis of the EPSPS sequences from a variety of fungi including the representative class I and II EPSPS sequences from *Vibrio cholerae* and *Coxiella burneti*, respectively (Fig. 1G). It revealed that the EPSPS enzymes of *Trichoderma* species—including *T. guizhouense*, *T. harzianum*, and *T. atroviride*—cluster within the class I group, suggesting their potential sensitivity to glyphosate. However, we failed to delete the EPSPS-encoding gene, probably due to the essential role of EPSPS in the shikimate pathway for the biosynthesis of the aromatic amino acids. Nevertheless, the resistance to R450 should be elevated by the overexpression of EPSPS. To test it, we overexpressed the EPSPS-encoding gene under the control of the *tef* promoter in *T. guizhouense*. However, the mutant strain showed no change in sensitivity to R450 (fig. S1A). In plants, glyphosate blocks the biosynthesis of three aromatic amino acids—L-phenylalanine (Phe), L-tyrosine (Tyr), and L-tryptophan (Try)—by targeting EPSPS (*21*), whereas the contents of these amino acids were not affected by the presence of R450 in the wild-type strain (fig. S1B). These results demonstrate that R450 does not target the EPSPS enzyme in *T. guizhouense*.

Triton CG-110 is more toxic than glyphosate

Next, we queried, except glyphosate, whether the additives in GBHs are toxic to fungi. The commonly used adjuvant Triton CG-110, an alkyl polyglycoside, has replaced POEA in Europe because of its toxicity to human cells (*24*–*26*). Therefore, we compared the effect of glyphosate and Triton CG-110 on the growth of *T. guizhouense*. Fungi can degrade glyphosate as a source of phosphorus, carbon, and nitrogen (*27*). We found that, instead of the inhibitory effect, glyphosate could promote vegetative growth, further confirming that glyphosate does not target EPSPS in *T. guizhouense*. However, Triton CG-110 inhibited the growth notably, indicating its higher toxicity than glyphosate (Fig. 1, H and I).

We observed that the inhibitory effect on growth was exacerbated slightly by the combination of Triton CG-110 and glyphosate (Fig. 1, H and I). In mammalian cells, the overaccumulation of glyphosate elevates the intracellular levels of reactive oxygen species (ROS) (*28*). We, therefore, hypothesized that the presence of Triton CG-110 could increase the intracellular accumulation of glyphosate and thus cause the increase of the hydrogen peroxide content in hyphae. To test this hypothesis, the intracellular glyphosate and hydrogen peroxide contents were measured. In comparison to the treatment with only glyphosate, the addition of Triton CG-110 led to a nearly tenfold increase of the glyphosate content in the mycelium (Fig. 1J), and consistently, the hydrogen peroxide content was also notably increased (Fig. 1K).

Overall, these results demonstrate that Triton CG-110 is the primary harmful factor for *T. guizhouense*. Moreover, it can facilitate cellular uptake of glyphosate, resulting in enhanced toxicity.

TMK1 pheromone pathway is implicated in Triton CG-110 response

Three MAPK signaling pathways—the pheromone pathway, the cell integrity pathway and the high osmolarity glycerol pathway corresponding to three *Trichoderma* MAP kinases TMK1, TMK2, and TMK3 (HOG1)—have been identified in *Trichoderma* species (*29*). Given the crucial role of the MAPK signaling pathways in regulating fungal environmental signal responses (*14*, *30*, *31*), we asked whether any of them were involved in the response of *T. guizhouense* to Triton CG-110. The wild-type, Δ*tmk1*, Δ*tmk2*, and Δ*hog1* strains were cultured with the potato dextrose agar (PDA) medium containing 0.075% Triton CG-110 for 48 hours. We found that the Δ*tmk1* strain was susceptible to Triton CG-110, suggesting the involvement of the TMK1 pheromone pathway (Fig. 2, A and B). Likewise, upon Triton GC-110 treatment, the conidial germination rate of the Δ*tmk1* strain was decreased notably in comparison to other strains (Fig. 2C). The colony edge images showed that the mycelium of the Δ*tmk1* strain appeared to be lysed, and it seemed that the cellular materials were fanned out at the tips of the hyphae (Fig. 2D). We further analyzed the TMK1 phosphorylation and the expression level of the *tmk1* gene upon Triton GC-110. Consistently, Western blot analysis indicated that Triton GC-110 treatment caused the phosphorylation of TMK1 (Fig. 2E), while real-time quantitative polymerase chain reaction (RT-qPCR) analysis showed that *tmk1* expression was not affected by the addition of Triton GC-110 (fig. S2). Similarly, we constructed a *tmk1* deletion strain in *T. harzianum*, which also showed sensitivity to Triton CG-110 (fig. S3). We further tested other non-ionic and ionic surfactants and found that only triton CG-110 caused notable growth inhibition of the Δ*tmk1* strain (fig. S4), suggesting the specificity of the pheromone pathway for Triton CG-110 response.

Identification of the components implicated in Triton CG-110 response

Next, we screened for the components up- and down-stream of TMK1. We first constructed the Δ*ste11* and Δ*ste7* strains corresponding to the MAPKKK STE11 and MAPKK STE7 in the TMK1 pheromone module, respectively. Both strains grew as slowly as the Δ*tmk1* mutant in the presence of Triton CG-110 (Fig. 2H).

GPCRs that can activate the pheromone pathway have been characterized in *Saccharomyces cerevisiae* (*16*). Using these GPCRs as queries, three potential upstream GPCR-encoding genes—termed *gpr1*, *gpr3* and *gpr4*—were identified by basic local alignment search tool (BLAST) searches in *T. guizhouense*. The corresponding mutants grew a little bit more slowly than the wild type in the presence of Triton CG-110 while still much faster than the Δ*tmk1* strain (Fig. 2, G to I). GPCRs signaling activates adenylyl cyclase, leading to increased production of intracellular cyclic adenosine 3′,5′-monophosphate (cAMP). cAMP can activate the pheromone pathway in *Ustilago*

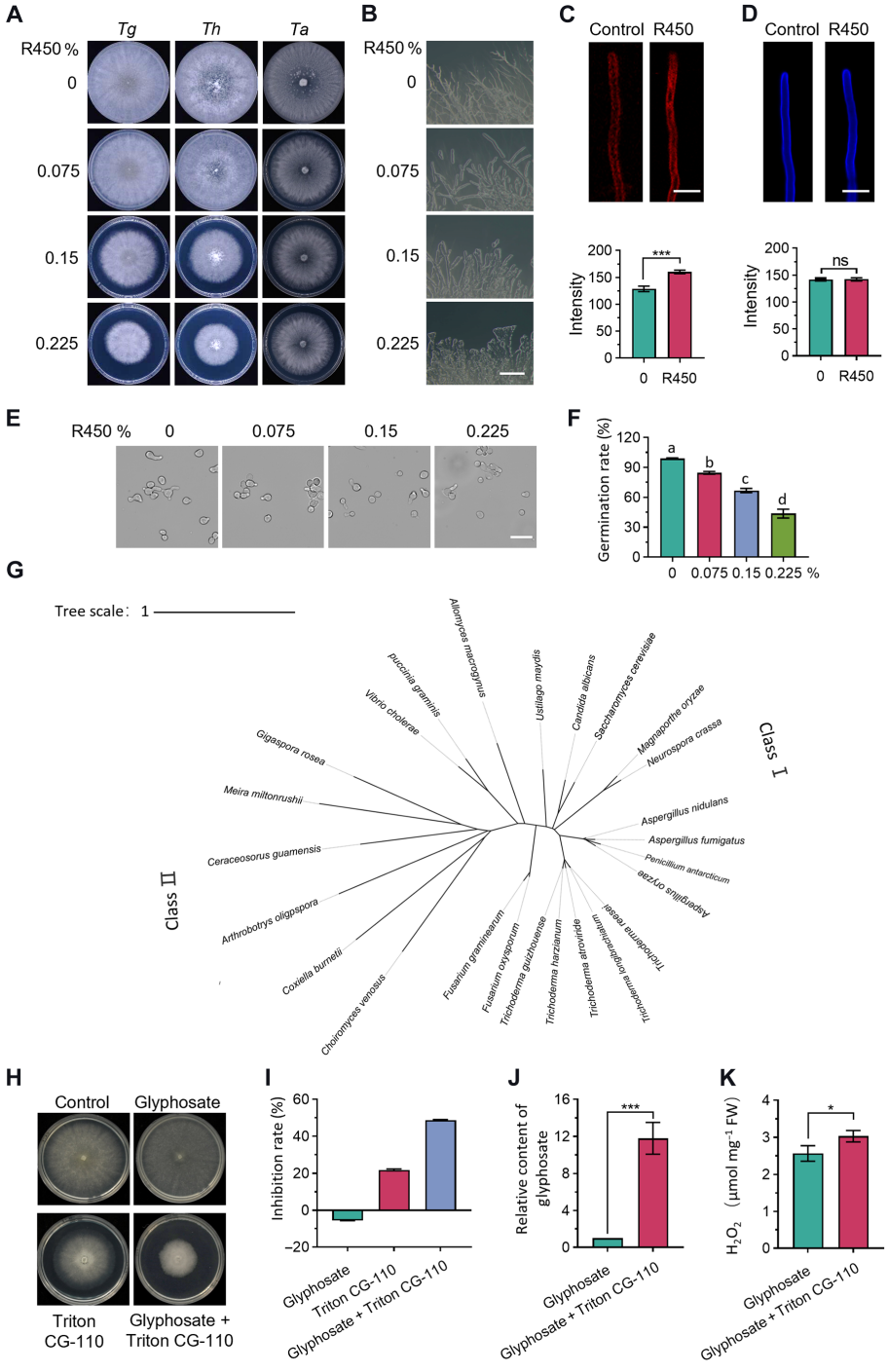

Fig. 1. Effects of R450, glyphosate, and Triton CG-110 on the growth of *Trichoderma* species. (**A**) Images of *T. guizhouenese* (*Tg*), *T. harzianum* (*Th*), and *T. atroviride* (*Ta*) grown on PDA plates containing R450. Each strain was incubated on PDA supplemented with 0, 0.075, 0.15, and 0.225% R450 at 25°C for 48 hours. (**B**) Effects of R450 on mycelia morphology. *T. guizhouense* was cultured on PDA at 25°C for 24 hours, and the colony edges were photographed using a stereoscopic microscope. Scale bar, 40 μM. (**C** and **D**) Florescent staining of cell membrane and cell wall. Fluorescent dyes of FM 4-64 and CFW were used for cell membrane and cell wall staining, respectively. Scale bars, 20 μm. Quantification of fluorescence intensity after staining using imageJ. $n = 3$. (**E**) Germination of conidia grown under different concentrations of R450. Scale bar, 20 μm. (**F**) Germination rates of conidia grown under different concentrations of R450. Data presented are means ± SD. $n = 3$. Different letters indicate significant differences at $P \leq 0.05$ according to one-way analysis of variance (ANOVA) and post hoc Duncan's test. (**G**) Phylogenetic tree of the EPSPS from different fungi was constructed using the neighbor-joining method. (**H** and **I**) Effects of glyphosate and Triton CG-110 on vegetative growth and conidia germination of *T. guizhouense*. Strain was incubated on PDA containing 0.075% Triton CG-110 and/or 4 mM glyphosate at 25°C for 48 hours. (**J**) Intracellular glyphosate content under Triton CG-110 treatment. Strain was cultured on PDA with glyphosate or glyphosate and 0.075% Triton CG-110 at 25°C for 48 hours. Data presented are means ± SD. $n = 3$. (**K**) Intracellular H_2O_2 content under Triton CG-110 treatment. Data presented are means ± SD. $n = 3$. [(C), (D), (J), and (K)] *P* value was calculated using a *t* test. $^*P \leq 0.05$, $^{***}P \leq 0.01$; ns, not significant.

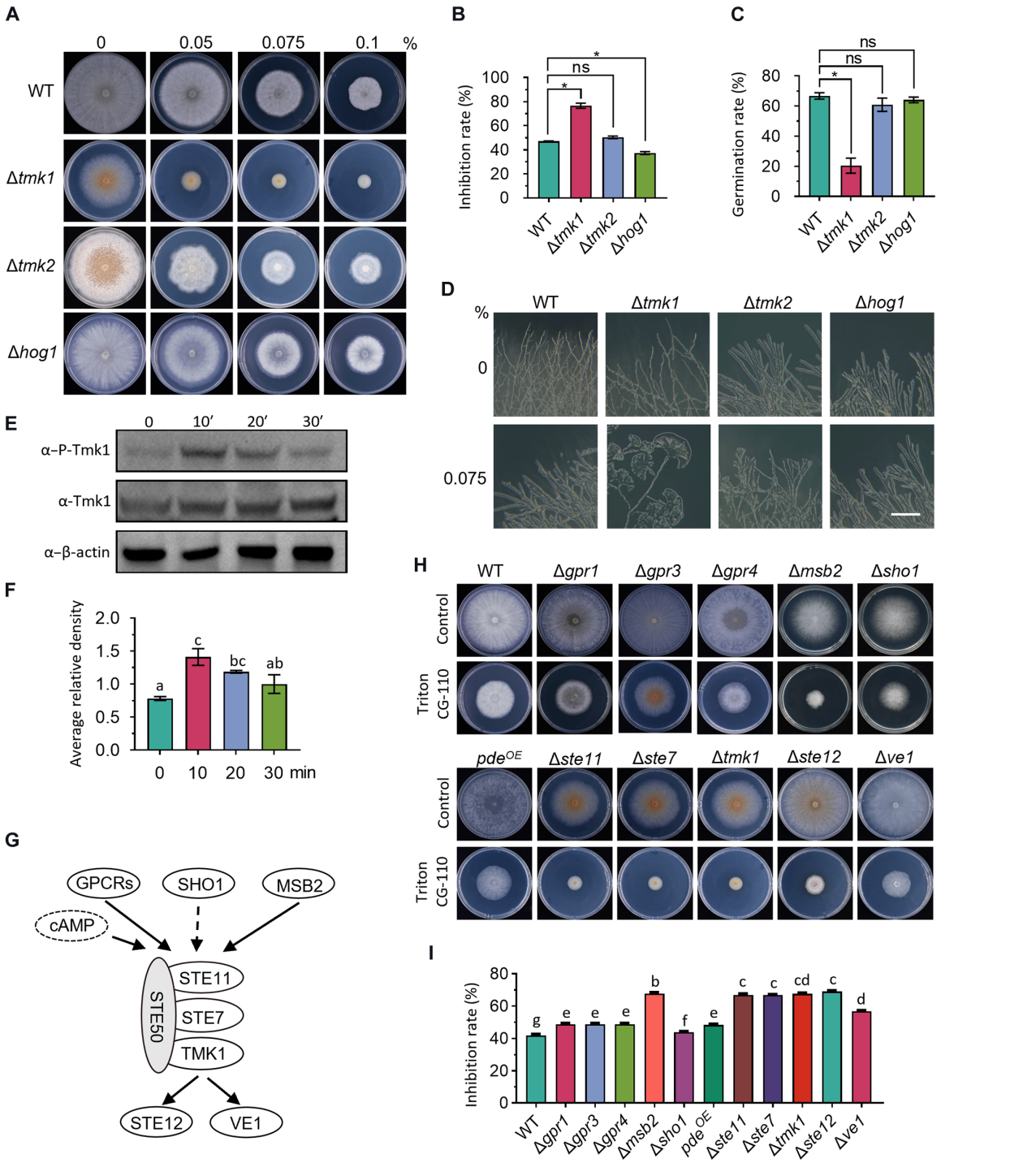

Fig. 2. The pheromone pathway responds to Triton CG-110 stimulation. (**A** and **B**) Growth phenotype of wild type, Δ*tmk1*, Δ*tmk2*, and Δ*hog1* mutants on PDA plates supplemented with different concentrations of Triton CG-110 at 25°C for 48 hours. The Δ*tmk1* mutant showed increased sensitivity to Triton CG-110. Data presented are means ± SD. $n = 3$. (**C**) Germination of wild-type spores after 12 hours of incubation in PDB containing 0.075% Triton CG-110. Data presented are the means ± SD. $n = 3$. (**D**) Mycelial morphology of wild-type, Δ*tmk1*, Δ*tmk2*, and Δ*hog1* mutants under Triton CG-110 treatment. The strains were cultured at 25°C for 48 hours and then photographed under a stereoscopic microscope. Scale bar, 10 μm. (**E** and **F**) Phosphorylation of TMK1 in response to Triton CG-110 treatment. A total of 1×10^5 wild-type spores were inoculated into PDB and cultured at 25°C and 180 rpm for 24 hours and then treated with Triton CG-110 for 10, 20, and 30 min. (**G**) Schematic model of fungal pheromone pathway. (**H** and **I**) Identification of the components of pheromone pathway involved in Triton CG-110 response. Wild-type and mutant strains deficient in *gpr1*, *gpr3*, *gpr4*, *msb2*, *sho1*, pde^{OE}, *ste11*, *ste7*, *tmk1*, *ste12*, and *ve1* were cultured on PDA or PDA containing 0.075% Triton CG-110 at 25°C for 48 hours, and the mycelial growth inhibition rate was calculated for each strain. Data presented are means ± SD. $n = 3$. [(B) and (C)] P value was calculated using a t test. $^*P \leq 0.05$. [(F) and (I)] Different letters indicate significant differences at $P \leq 0.05$ according to one-way ANOVA and post-hoc Duncan's test.

maydis, which can be hydrolyzed by the phosphodiesterase (PDE) (*32*). Therefore, we tested whether the overexpression of *pde* could increase the sensitivity to Triton CG-110. The sensitivity of the overexpression strain (pde^{OE}) to Triton CG-110 was only increased slightly compared to the wild type, suggesting that three GPCRs and cAMP do not play a pivotal role in this case (Fig. 2H).

In plant pathogenic fungi—*Magnaporthe oryzae*, *U. maydis*, and *Fusarium oxysporum*—the signaling mucin Msb2 and the plasma membrane-spanning protein Sho1 can recognize surface signals to activate the pheromone pathway (*33*–*35*). We identified their homologous proteins in *T. guizhouense* and constructed the corresponding deletion mutants Δ*msb2* and Δ*sho1*. The Δ*msb2* strain exhibited the same sensitivity to Triton CG-110 as the Δ*tmk1* strain.

In *Aspergillus nidulans*, the downstream transcription factors of the pheromone pathway are SteA-regulating vegetative growth, cell fusion, asexual and sexual development, and VeA crucial for secondary metabolism (*12*). The genes encoding their orthologs STE12 and VE1 in *T. guizhouense* were deleted, and only the Δ*ste12* strain has the same phenotype as the Δ*tmk1* mutant in the presence of Triton CG-110 (Fig. 2H). In summary, these results demonstrate a clear signal transduction pathway from the receptor MSB2 to the TMK1 pheromone module and then to the transcription factor STE12 in response to Triton CG-110.

Triton CG-110 regulates membrane and steroid biosynthesis genes

Next, we investigated the transcriptomic profiles of the wild type and Δ*tmk1* strains grown on the medium with or without Triton CG-110. In the presence of Triton CG-110, 443 genes in wild type were differentially expressed ($|\log_2(\text{fold change})| \geq 1$, $P \leq 0.05$) and 66.4% (294 of 443) of these differentially expressed genes (DEGs) were regulated by the TMK1 pheromone pathway (Fig. 3A). The Kyoto Encyclopedia of Genes and Genomes (KEGG) pathway and Gene Ontology (GO) functional enrichment analyses were performed on the basis of the DEGs identified in the wild-type strain. The GO analysis revealed a notable enrichment of these genes in the terms related to cell structure, specifically in the cell wall and membrane terms. We analyzed the cell wall–related genes within the cell wall term and identified 25 genes in total, of which 6 (24%) were differentially expressed, primarily associated with chitinase and hydrophobins. However, crucial enzymes for cell wall structure, such as β-glucan and chitin synthases, were not differentially expressed. Steroids and fatty acids are integral to the eukaryotic cell membrane, playing crucial roles in regulating membrane fluidity and permeability (*19*). While fatty acid biosynthesis genes showed no notable differential expression (fig. S6), steroid biosynthesis was one of the top 12 enriched pathways in the KEGG analysis with *erg6A* and *erg6B* being the most highly up-regulated genes (Fig. 3, B and C).

STE12 mediates plasma membrane integrity by regulating ergosterol biosynthesis

In *A. nidulans*, *S. cerevisiae,* and *M. oryzae*, the orthologs of TMK1 interact with the orthologs of STE12 to regulate gene expression (*12*, *36*). To confirm the interaction between TMK1 and STE12, STE12 was labeled with green fluorescent protein (GFP). Co-immunoprecipitation (Co-IP) assay, performed with the antibodies against GFP and TMK1, indicated the interaction between STE12 and TMK1 (fig. S5). We further analyzed the transcriptomes of the wild-type, Δ*tmk1*, and Δ*ste12* strains, which revealed that 908 DEGs were coregulated by TMK1 and STE12. The GO functional enrichment analysis of these DEGs resulted in a notable enrichment in the cell membrane term (111 of 908, $P = 0.000023$), indicating the regulatory role of TMK1 and STE12 for cell membrane (Fig. 3, D and E).

Plasma membrane integrity (PMI) is vital for cell survival and function (*37*). To analyze the effect of Triton CG-110 treatment on PMI, we stained the germlings with propidium iodide (PI) and Hoechst to assess membrane integrity. In the presence of Triton CG-110, we observed a notable increase in PI fluorescence signal particularly in the Δ*tmk1* and Δ*ste12* strains (Fig. 3F), suggesting increased plasma membrane damage. To further evaluate PMI, PI staining of protoplasts combined with the fluorescence-activated cell sorting approach was conducted. Before treatment, there was no notable difference in PI fluorescence intensity between different strains, but upon Triton CG-110 treatment the fluorescence intensity in the Δ*tmk1* and Δ*ste12* strains was notably higher than that of the wild-type strain (Fig. 3, G to J). Evan's blue was used to examine PM stability. Spectrophotometry quantitation showed that the Δ*tmk1* and Δ*ste12* strains exhibited a higher stain content than the wild-type strain after Triton CG-110 treatment (Fig. 3K). These indicate notable changes of PMI in the Δ*tmk1* and Δ*ste12* strains upon Triton CG-110 treatment.

Because ergosterol is the major sterol of fungal cell membrane and critical for membrane integrity and stability, we measured the content of ergosterol in the wild-type, Δ*tmk1*, and Δ*ste12* strains. Ergosterol content in wild-type strain was increased after the treatment, while in the Δ*tmk1* and Δ*ste12* strains, it was markedly decreased (Fig. 3L), indicating the impaired ergosterol biosynthesis in the Δ*tmk1* and Δ*ste12* strains upon Triton CG-110 treatment. These results demonstrate that STE12 and TMK1 regulate PMI by controlling ergosterol biosynthesis.

STE12 binds to the promoters of ergosterol biosynthesis genes

Ergosterol biosynthesis in fungi involves multiple biochemical reactions that convert acetyl-CoA to ergosterol (*19*). In *T. guizhouense*, 25 ergosterol biosynthesis genes (*ergs*) were identified by BLAST searches based on *ergs* in yeast. Transcriptomic analysis revealed notable upregulation of most *ergs* in the wild-type strain upon Triton CG-110 treatment, which, however, was not the case in the Δ*tmk1* strain, suggesting that a regulatory mechanism relies on *tmk1* (Fig. 4A). RT-qPCR analyses further confirmed that *erg6A*, *erg6B*, *erg7*, *erg11*, *erg20A*, and *erg24B* were under the control of TMK1 and STE12 (fig. S7 and Fig. 4B).

In addition, we performed gene knockouts of *erg6A*, *erg6B*, *erg7*, *erg11*, and *erg24B*, which were differentially expressed ($|\log_2(\text{fold change})| \geq 1$, $P \leq 0.05$) after Triton CG-110 treatment. All the genes were knocked out except *erg7*, which might be essential. Given the functional redundancy of *erg6A* and *erg6B* in converting zymosterol to fecosterol (*37*), a double knockout strain Δ*erg6A*Δ*erg6B* was also created. These mutants—especially Δ*erg6A*, Δ*erg11*, Δ*erg24A* and Δ*erg6A*Δ*erg6B*—exhibited increased sensitivity to Triton CG-110, demonstrating the involvement of ergosterol synthesis (Fig. 4, C and D).

To evaluate the direct regulatory relationship between the transcription factor STE12 and *ergs*, yeast one-hybrid (Y1H) assays were performed. Y1H assays showed that STE12 directly bound to the 1-kb promoter regions of *erg6A*, *erg6B*, *erg7*, *erg11*, and *erg24B* (Fig. 4E). In *M. oryzae*, the STE12 ortholog Mst12 putatively binds

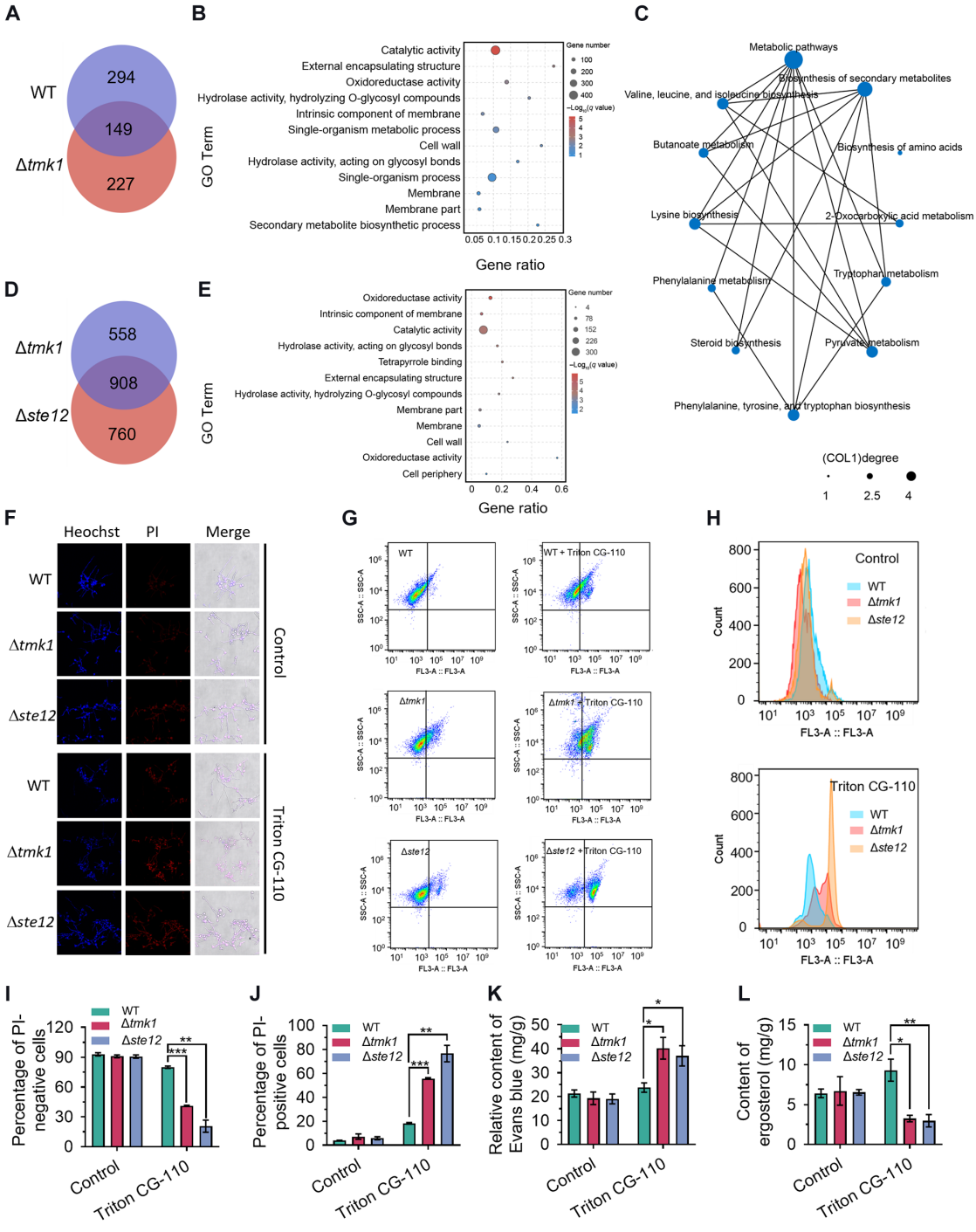

Fig. 3. PMI of *T. guizhouense* in response to Triton CG-110 treatment by the regulation of TMK1 and STE12. (**A**) Venn Diagram of DEGs in *T. guizhouense* in response to Triton CG-110 treatment. The strains were cultured on PDA containing 0.075% Triton CG-110 at 25°C for 24 hours. (**B** and **C**) GO and KEGG pathway enrichment analysis of DEGs exposed to Triton CG-110. Each diagram represents the top 12 pathways based on the enrichment significance. (**D**) Venn diagram analysis of the DEGs in Δ*tmk1* and Δ*ste12* mutants. (**E**) GO enrichment analysis of coregulated DEGs of *tmk1* and *ste12* exposed to Triton CG-110. (**F**) Staining of the germlings Hoechst and propidium iodide (PI) upon Triton CG-110 treatment. (**G** to **J**) PI staining and fluorescence-activated cell sorting (FACS) analyses of protoplasts from wild-type, Δ*tmk1*, and Δ*ste12* strains before and after exposure to Triton CG-110. The protoplasts were treated with 0.075% Triton-CG 110 for 10 min and then stained with 10 mM PI for 15 min. SSC-A, side scatter area. $n = 3$. Percentage of PI-positive and PI-negative cells was shown. Data presented are means ± SD. $n = 3$. (**K**) Quantification of plasma membrane stability through Evan's blue assay. Strains were incubated with Evan's blue solution for 15 min and subsequently lysed using SDS, followed by centrifugation. Data presented are means ± SD. $n = 3$. (**L**) Ergosterol content analysis in wild-type, Δ*tmk1*, and Δ*ste12* strains. A total of 1×10^5 spores were inoculated into PDB or PDB containing 0.075% Triton CG-110 and cultured at 25°C and 180 rpm for 24 hours. Data presented are means ± SD. $n = 3$. (**I** to L) *P* value was calculated using a *t* test. $^*P \leq 0.05$, $^{**}P \leq 0.01$, and $^{***}P \leq 0.01$.

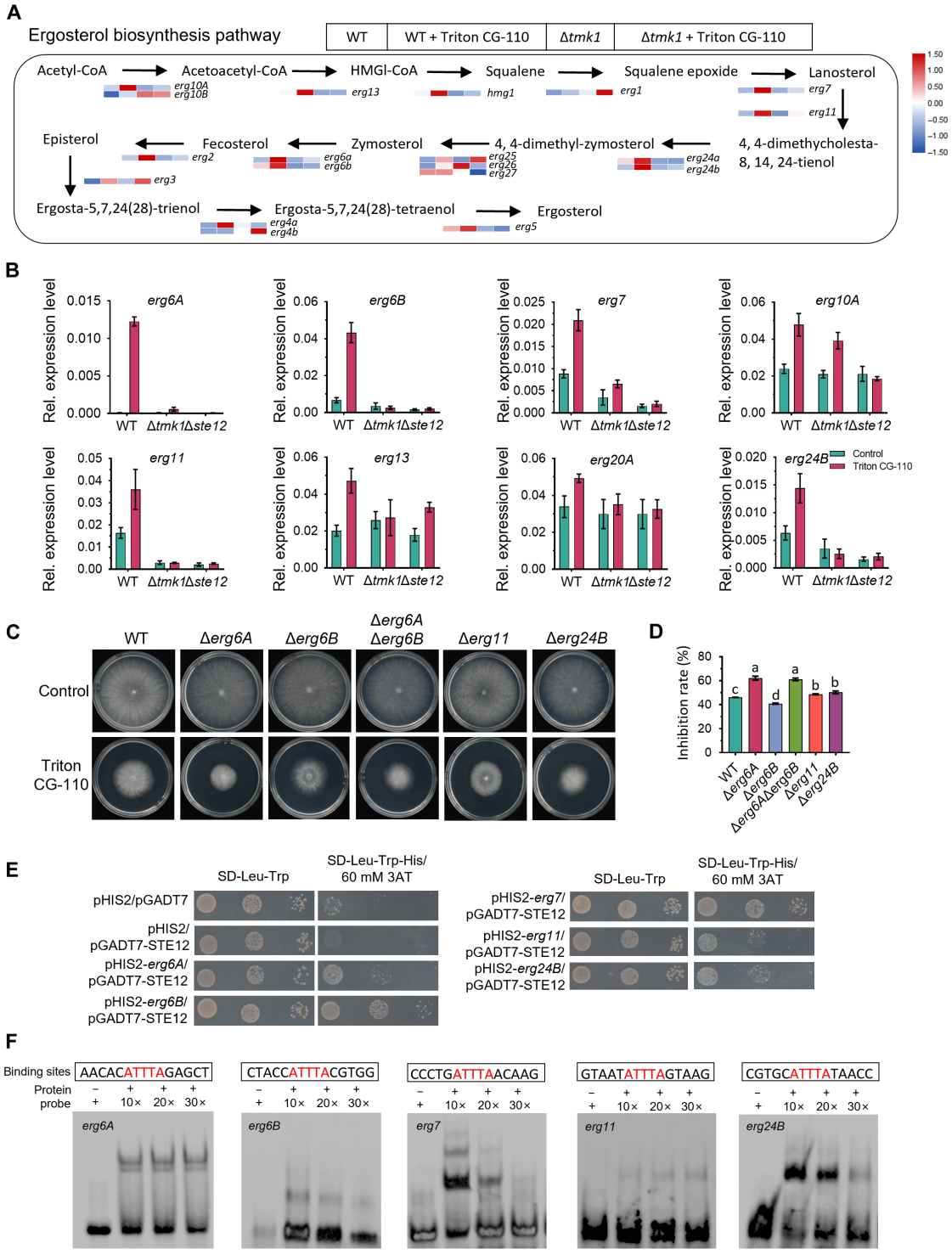

Fig. 4. Regulatory of *tmk1* and *ste12* on ergosterol biosynthesis genes in *T. guizhouense*. (**A**) Transcriptome analyses of ergosterol biosynthesis genes (*ergs*) in *T. guizhouense* under Triton CG-110 treatment. The fragment per kilobase of transcript per million mapped reads (FPKM) values of *ergs* were used to create the heatmap with the Complex Heatmap package in RStudio. (**B**) Expression levels of *ergs* in the wild-type, Δ*tmk1*, and Δ*ste12* strains. All strains were grown on PDA and PDA with 0.075% Triton CG-110 at 25°C for 24 hours. The total RNA was extracted from four separate cultures. Expression levels were normalized to the reference gene *tef1*. Data presented are means ± SD. $n = 3$. (**C**) Effect of Triton CG-110 on mycelial growth in the *ergs* deletion strains. The strains were cultured on PDA or PDA containing 0.075% Triton CG-110 at 25°C for 48 hours. Data presented are means ± SD. $n = 3$. (**D**) Inhibition rates of strains in (C). The mycelial growth inhibition was calculated for each strain. Data presented are means ± SD. $n = 3$. Different letters indicate significant differences at $P \leq 0.05$ according to one-way ANOVA and post hoc Duncan's test. (**E**) STE12 binds to the promoter of *ergs* in Y1H assays. The native ~1-kb promoter of *ergs* was used as bait and the pGADT7-STE12 as the prey. (**F**) Verification of the binding of STE12 with the cis-element by EMSA. Lane 1, a biotin-labeled motif of *ergs* without STE12; lane 2 to 4, dilute the 10 nM biotin-labeled motif 10, 20, and 30 times with STE12.

to several motifs identified by ChIP sequencing to regulate appressorium maturation and plant infection (*36*). On the basis of these DNA binding motifs of Mst12, we conducted a comparative sequence analysis of these gene promoters to identify cis-elements targeted by STE12. This analysis revealed a putative cis-element containing the 5′-ATTTA-3′ sequence. Recombinant protein of STE12 was expressed in *Escherichia coli* and purified for electrophoretic mobility shift assay (EMSA), which confirmed the binding of STE12 to the region containing the above motif (Fig. 4F and fig. S8).

Shedding of MSB2 activates the TMK1 pheromone pathway

The growth of the Δ*msb2* strain was notably inhibited by Triton CG-110, suggesting the roles of MSB2 in Triton CG-110 sensing and TMK1 pheromone pathway activation. In addition, PI fluorescence intensity of Δ*msb2* was similar to that of Δ*tmk1* upon Triton CG-110 treatment (fig. S9). To confirm the activation of TMK1 pheromone pathway by MSB2 under Triton CG-110 treatment, we analyzed the phosphorylation of TMK1 in the wild-type and Δ*msb2* strains and found that the phosphorylation level of TMK1 in the Δ*msb2* strain remained unchanged in comparison to that in the wild-type strain (Fig. 5, A and B).

Msb2, as a signaling mucin, has a single transmembrane region that divides the protein into a large glycosylated extracellular domain and a small cytoplasmic domain. In *S. cerevisiae*, the extracellular domain of Msb2p ortholog MSB2 sheds from the plasma membrane under the catalysis of the aspartyl protease Yps1p (*38*, *39*). The presence

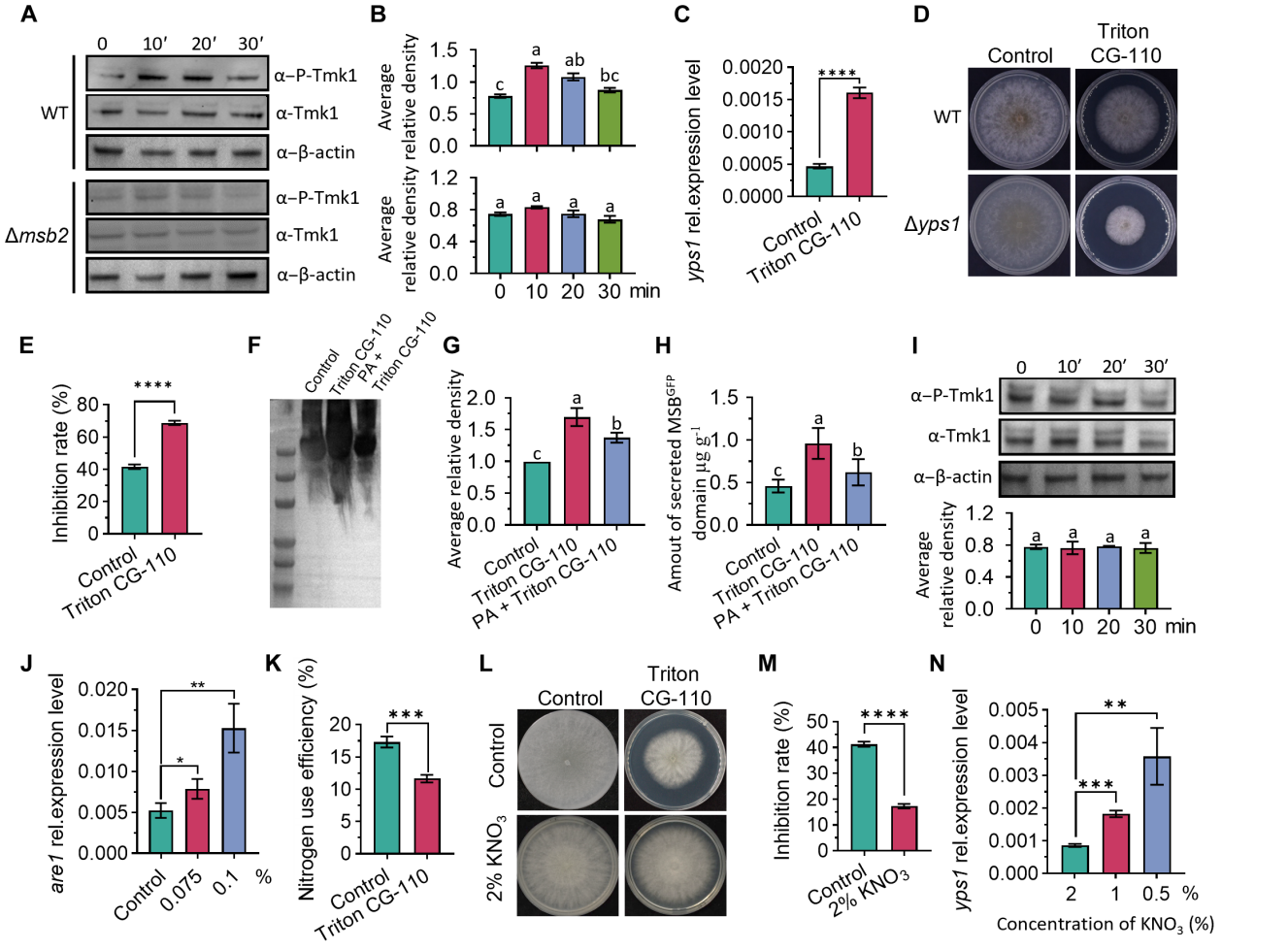

Fig. 5. MSB2 activates TMK1 by regulating shed through YPS1 under nitration limitation. (**A** and **B**) Phosphorylation of TMK1 in response to Triton CG-110 treatment in wild-type and Δ*msb2* strains. The average relative density was quantified using ImageJ. $n = 3$. (**C**) Relative expression level of *yps1* under Triton CG-110 treatment. Expression levels were normalized to the reference gene *tef1*. Data presented are means ± SD. $n = 3$. (**D** and **E**) Effect of Triton CG-110 on mycelial growth in the Δ*yps1* strain. Data presented are means ± SD. $n = 3$. (**F** and **G**) Secretion of GFP-tagged MSB2 protein during growth under Triton CG-110 treatment. Secretion of GFP-tagged MSB2 was purified by affinity chromatography. The average relative density was quantified using ImageJ. $n = 3$. (**H**) Quantification of GFP in secreted $MSB2^{GFP}$ domain using enzyme-linked immunosorbent assay, normalized to the fresh weight of the mycelium. (**I**) Phosphorylation of TMK1 in response to Triton CG-110 and PA treatment. The average relative density was quantified using ImageJ. $n = 3$. (**J**) Relative expression level of *are1* under Triton CG-110 treatment. Expression levels were normalized to the reference gene *tef1*. Data presented are means ± SD. $n = 3$. (**K**) Nitrogen use efficiency of wild type under Triton CG-110. Data presented are means ± SD. $n = 3$. (**L** and **M**) Effect of NO_3^- on wild type under Triton CG-110 treatment. Data presented are means ± SD. $n = 3$. (**N**) Relative expression level of *yps1* under various concentrations of KNO_3. Expression levels were normalized to the reference gene *tef1*. Data presented are means ± SD. $n = 3$. [(C), (E), (J), (K), (M), and (N)] *P* value was calculated using a *t* test. $^*P \le 0.05$, $^{**}P \le 0.01$, and $^{***}P \le 0.01$. [(B), (G), (H), and (I)] Different letters indicate significant differences at $P \le 0.05$ according to one-way ANOVA and post hoc Duncan's test.

of Triton CG-110 up-regulated the expression of the Yps1p ortholog-encoding gene, *yps1*, in *T. guizhouense* (Fig. 5C), and moreover, the *yps1* deletion notably increased the sensitivity of the strain to Triton CG-110 (Fig. 5, D and E). Therefore, we hypothesized that Triton CG-110 could promote the shedding of MSB2 extracellular domain from the plasma membrane, thereby leading to the phosphorylation of TMK1. To test this hypothesis, we fused a GFP to the extracellular region of MSB2 in *T. guizhouense*, and thus, it could be enriched using anti-GFP magnetic beads. The GFP-labeled strain was cultured in potato dextrose broth (PDB) medium with or without Triton CG-110. The extracellular domain shed into the medium was enriched and analyzed by Western blot. As shown in Fig. 5 (F to H), in the presence of Triton CG-110, more MSB2 extracellular domains were detected in the medium. Consistently, in the presence of the specific aspartic protease inhibitor (PA), shedding of the MSB2 extracellular domain was reduced. PA inhibited the potential protease activity to reduce the cleavage of MSB2. Furthermore, we found that the phosphorylation level of TMK1 did not change upon Triton CG-110 treatment when PA was present (Fig. 5I). These results demonstrate that the shedding of the MSB2 extracellular domain activates the pheromone pathway under Triton CG-110 treatment.

Triton CG-110 induces *yps1* expression by limiting nitrogen uptake

Nitrogen uptake relies on membrane potential maintenance, and plasma membrane damage disrupts electrochemical gradients, hindering active nitrogen uptake (*40*). AreA is a global transcription factor regulating genes involved in nitrogen uptake, transport, and catabolism in filamentous fungi and induced under nitrogen-limited conditions (*41*). We found that the *are1* gene encoding a homolog of the *Aspergillus niger* AreA was up-regulated notably under the Triton CG-110 treatment (Fig. 5J). Moreover, nutrition limitation can increase Yps1p expression in *S. cerevisiae*, which is the primary Yps protease required for shedding of Msb2p (*39*). We then speculated that Triton CG-110 treatment might impair the uptake of nitrogen source, leading to the up-regulation of the *yps1* gene expression. Therefore, we cultured the wild-type strain with the PDA medium supplemented with 1% ^{15}N-labeled KNO_3. The nitrogen use efficiency was notably decreased in the presence of Triton CG-110 (Fig. 5K). Consistently, supplementation of 2% KNO_3 in the PDA medium attenuated the inhibitory effect of Triton CG-110 on the vegetative growth (Fig. 5, L and M). To confirm that nitrogen limitation can induce *yps1* expression, the wild-type strain was cultured in the medium supplemented with varying proportions of KNO_3. RT-qPCR analysis indicated that *yps1* expression was increased with the decrease of the KNO_3 proportion (Fig. 5N). These results demonstrate that Triton CG-110 can restrict nitrogen uptake in *T. guizhouense*, leading to the induction of *yps1* expression.

DISCUSSION

Although soil microorganisms can degrade glyphosate, the main active constituent of GBHs, a large body of literature highlights the negative effects of GBHs on soil fungi. In this study, we found that R450 impairs the hyphal growth and conidial germination of *Trichoderma* species and further found that the herbicide adjuvant Triton CG-110 is more toxic than glyphosate to fungal cells. We demonstrate that Triton CG-110 exposure leads to restricted nitrogen uptake, which induces the expression of the aspartyl proteinase-encoding gene YPS1 (Fig. 6). YPS1 catalyzes the cleavage of MSB2, resulting in the activation of the TMK1 pheromone pathway. Phosphorylated TMK1 interacts with STE12 that directly regulates ergosterol biosynthesis, affecting membrane fluidity and stability. Nutrient uptake primarily relies on cell membrane transporters and the integrity of the cell membrane is paramount, as it regulates the passage of essential nutrients and ions. We speculate that the change of PMI caused by Triton CG-110 exposure impairs the functions of those cell membrane transporters, thereby reducing nitrogen use efficiency, which induces the expression of *yps1*. In addition to its own cytotoxicity, Triton CG-110 causes the overaccumulation of intracellular glyphosate and thus elevates intracellular ROS levels. The cellular toxicity caused by the accumulation of glyphosate with the aid of the adjuvant should also not be overlooked. On the other hand, the sensitivity of the *T. harzianum tmk1* deletion strain to Triton CG-110 treatment suggests that other filamentous fungi may also use the same mechanism to sense Triton CG-110 signal.

In fungi, 92% of the EPSPS enzymes belong to class I (*2*), which are probably sensitive to glyphosate due to the absence of the residues essential for glyphosate resistance commonly found in class II. However, to our knowledge, there is still no wet lab experimental evidence that glyphosate can target the shikimate pathway in fungi. Likewise, we demonstrate that, although EPSPS in *T. guizhouense* was classified into class I, R450 does not target the shikimate pathway in *T. guizhouense*. EPSPS in *A. nidulans* is also classified into class I, whereas R450, rather than the pure glyphosate, inhibits the vegetative growth (*6*). Therefore, if the class I EPSPS enzymes in other fungi are targeted by glyphosate, then it is worthy of further investigation.

It is unexpected that ergosterol biosynthesis and PMI are regulated by the MSB2-mediated pheromone pathway. It is known that ergosterol biosynthesis in most fungi and cholesterol biosynthesis in mammals are regulated by the membrane-bound transcription factor SREBP (*19*, *42*). Cleaved by the DSC complex and rhomboid protease, SREBP releases the N-terminal transcriptional activation domain to the cytoplasm, which can translocate into the nucleus to regulate ergosterol or cholesterol biosynthesis genes. In addition, another membrane-bound transcription factor Upc2, tethered to the membrane through its ergosterol-binding domain, is released under ergosterol-depleted conditions and then translocates into the nucleus to regulate ergosterol biosynthesis in *S. cerevisiae* (*43*). However, the pheromone pathway seems not associated with SREBP and Upc2. While the filamentous fungus *Aspergillus fumigatus* encoding two orthologs of SEEBP, SrbA and SrbB (*19*), in *T. guizhouense* we only found the SrbA ortholog, named SRB1. It belongs to the basic helix-loop-helix (HLH) family of transcription factors and has no high similarity with STE12 in its DNA binding domain. STE12 in *S. cerevisiae* targets a 5′-(A)TGAAACA-3′ motif, known as the pheromone response element (PRE) (*44*), whereas similar motifs were not found in the promoters of *ergs* and the *T. guizhouense* STE12 binds to a distinct motif of 5′-ATTTA-3′.

In conclusion, our study unravels how the MSB-mediated pheromone pathway regulates fungal PMI and emphasizes the necessity to re-evaluate the side effects of herbicides from the aspect of adjuvants. The impact of the adjuvants on soil microorganisms is worthy of concern.

MATERIALS AND METHODS

Strains, media, and culture conditions

Strains used in this study were listed in table S1. *T. guizhouense* NJAU4742 and its transformants were cultured at 25°C on PDA or

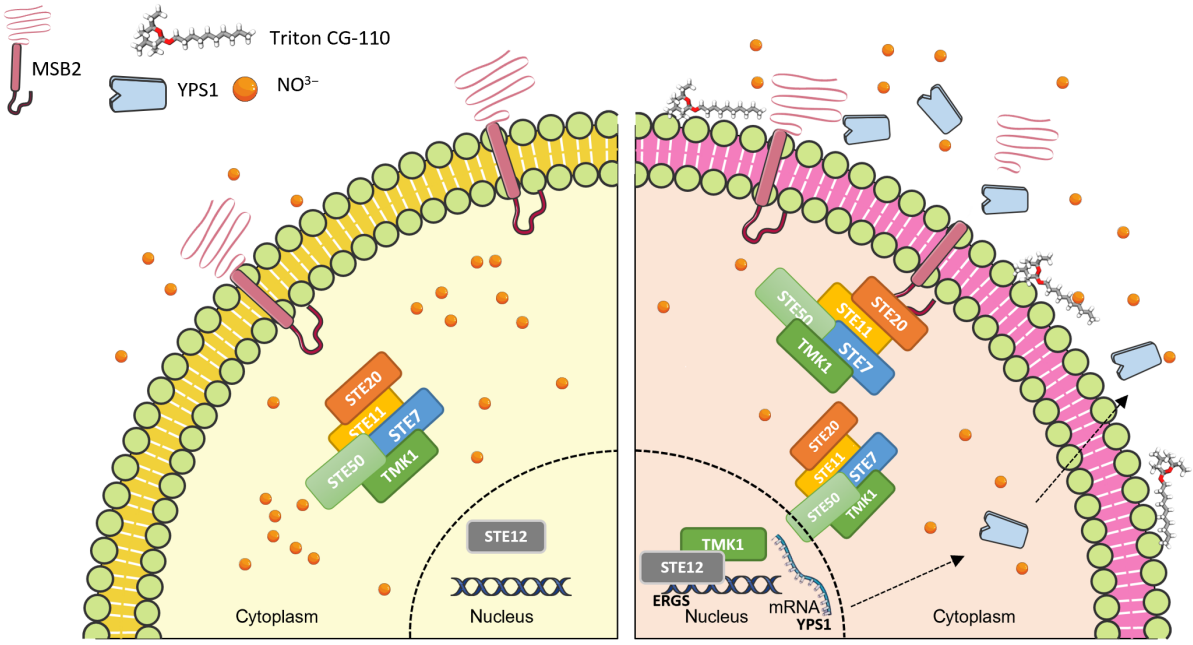

Fig. 6. A proposed model of *T. guizhouense* under Triton CG-110 treatment. Upon exposure to Triton CG-110, *T. guizhouense* encounters nitrogen limitation, prompting the up-regulation of the aspartic protease *yps1*. This promotes the cleavage and activation of the transmembrane protein MSB2, subsequently initiating the pheromone pathway. Furthermore, downstream STE12 can interact with the promoters of multiple ergosterol biosynthesis genes, thereby preserving the PMI of *T. guizhouense* in response to Triton CG-110 treatment.

in PDB. *E. coli* DH5α and BL21 were used for plasmid construction and protein expression in LB medium with appropriate antibiotics, respectively. *S. cerevisiae* Y187 and its transformants were grown at 30°C on yeast peptone dextrose adenine (YPDA) medium.

Strain construction

To construct plasmids and linear DNA fragments, ClonExpress MultiS One Step Cloning Kit (Vazyme, China) and 2× Phanta Max Master Mix (Dye Plus) (Vazyme, China) were used. PCR amplifications were performed on Thermo Fisher ProFlex PCR according to the standard instructions of different polymerases.

To obtain deletion mutants of corresponding genes, ~1.5-kb upstream and downstream fragments of target genes were amplified from *T. guizhouese* genomic DNA. The hygromycin B phosphotransferase–(*hph*) and neomycin phosphotransferase–(*neo*) encoding genes were used as the selective marker genes. The deletion cassettes of targeted genes were constructed by homologous recombination. To construct STE12-eGFP strains, ~1.5-kb upstream and downstream fragments of the stop codon of targeted genes and the cassettes with *eGFP* and *hph* were inserted into the pUC19. All plasmids were verified by PCR. Primers used in this study are listed in table S2, respectively. Each deletion cassette and *gfp* cassette was transformed into *T. guizhouense* strain according to a polyethylene glycol–mediated protoplast transformation method described previously.

Phenotypic analysis of different strains

T. guizhouense and its mutants were cultured on PDA containing Triton CG-110 or glyphosate-based herbicide at 25°C for 48 hours. The hyphae at the colony edge were photographed under a stereoscopic microscope. Each experiment was conducted in three biological replicates. To analyze the conidial germination, fresh conidia (1×10^5 spores per plate) were spread on PDA plates and incubated for 12 hours in the dark. Conidial germination was observed under a microscope.

Determination of glyphosate content by LC-MS/MS

Wild type was cultured on PDA containing 4 mM glyphosate or 4 mM glyphosate and 0.075% Triton CG-110 at 25°C for 48 hours. The 1 g of sample was then soaked in 15 ml of ultrapure water for 30 min before adding 10 ml of dichloromethane. The mixture was centrifuged at 4000 rpm for 10 min. The aqueous layer was transferred to another tube, and the process was repeated by adding another 15 ml of water to the residue for a second extraction. The combined aqueous solutions were thoroughly mixed. A C18 SPE column was activated sequentially with 5 ml of acetonitrile and 5 ml of water. For derivatization, 1 ml of the purified sample was mixed with 200 μl of 5% borate buffer and 200 μl of a Fmoc-Cl (30 g/liter) in acetone solution. The mixture was incubated at 30°C in the dark for 6 hours. The derivatized solution was then filtered through a 0.45-μm aqueous phase filter. The samples were separated by liquid chromatography tandem mass chromatography (LC-MS/MS) on a ZORBAX Eclipse Plis C18 column (2.1 mm by 150 mm, 3.5 μm) with a mobile phase consisting of 95% methanol and 5% water. Each sample was prepared in triplicate.

Total RNA extraction and RT-qPCR

To detect the expression levels of *ergs*, fresh mycelia were inoculated on PDA or PDA containing 0.075% Triton CG-110 covered with cellophane in 6-cm petri dishes and incubated at 25°C for 24 hours in the dark. To detect the expression level of *yps1*, fresh mycelia were inoculated on glucose synthetic medium (GSM) containing 0.5, 1, and 2% KNO_3 covered with cellophane in 6-cm petri dishes and

incubated at 25°C for 24 hours in the dark. Subsequently, the mycelia were harvested and frozen in liquid nitrogen for RNA isolation immediately.

Total RNA extraction was conducted utilizing the SteadyPure Plant RNA Extraction Kit (Accurate Biotechnology, China). Thereafter, 1 μg of total RNA was used for cDNA synthesis using the HiScript II Q RT SuperMix for qPCR (Vazyme, China). qRT-PCR was carried out using the qPCR SYBR Green Master Mix (Yeasen, China) on a qTOWER 2.2 system (Jena, Germany). The *tef* gene served as the reference for normalization. All statistical analyses were based on data obtained from four independent biological replicates.

Transcriptome sequencing

T. guizhouense and its mutants were incubated on PDA or PDA containing 0.075% Triton CG-110 covered with cellophane in 6-cm petri dishes at 25°C in the dark for 24 hours. The mycelium was harvested and frozen immediately in liquid nitrogen. Transcriptome sequencing was conducted using the Novaseq platform by Gene Denovo Biotechnology (Guangzhou, China). Each experimental group comprised three independent biological replicates for transcriptome sequencing.

Following stringent quality control measures, clean reads were aligned to the reference genome of *T. guizhouense* using HASAT2 v2.1.0. RNA sequencing (RNA-seq) alignment of potential transcripts is assembled by StringTie v1.3.1, with the calculation of fragment per kilobase of transcript per million mapped reads values. DEGs were identified using DEGseq2 with the thresholds of $|\log_2(\text{fold change})| \geq 1$ and false discovery rate ≤ 0.05. The gplots package was used for the expression enrichment analysis of DEGs, and the ClusterProfiler package v3.0.5 was used for their functional annotation. The RNA-seq data are available in the National Center for Biotechnology Information Sequencing Read Archive (SRA) (accession no. PRJNA1202995).

Protein extraction and immunoblot detection

Fresh conidia were inoculated into 50 ml of PDB and cultured at 25°C for 24 hours, and then, 0.075% Triton CG-110 was added. The mycelia were harvested at 10, 20, and 30 min after adding Triton CG-110 and frozen in liquid nitrogen immediately for protein extraction. After separation, proteins were transferred to polyvinylidene difluoride membranes. The immunoblotting was performed following the standard procedure with the anti–phospho-p44/42 MAP kinase antibodies, anti-p44/42 antibodies (Cell Signaling Technology, USA), and horseradish peroxidase (HRP)–conjugated monoclonal antibody (Yeasen, China) at the dilution of 1:1000. To normalize protein levels, β-actin (Abmart, China) was used as a loading control. Each experiment was repeated three times, and protein band intensities were quantified using ImageJ.

The secreted $MSB2^{GFP}$ domain was purified by affinity chromatography from the culture grown in PDB, PDB containing 0.075% Triton CG-110 and PDB containing 0.075% Triton CG-110, and 10 mM PA using BeyoMag Anti-GFP Magnetic Beads. Following three times of washing with PBS, the beads were resuspended in SDS–polyacrylamide gel electrophoresis loading buffer and heated at 95°C for 5 min to elute the proteins. The immunoblotting was performed following the standard procedure with the anti-GFP antibodies and HRP-conjugated monoclonal antibody (Yeasen, China) at the dilution of 1:1000. The amount of GFP in the purified secreted MSB^{GFP} domain was further quantified using a GFP ELISA kit (Abcam, England). Absorbance was measured at 450 nm using a microplate reader, and the protein quantity was normalized to the fresh weight of the mycelium to ensure comparability between samples.

Co-IP assay

To explore the in vivo interaction between TMK1 and STE12, a STE12-GFP strain was generated. Fresh spores (1×10^5) were inoculated into 50 ml of PDB medium and incubated in a shaking incubator at 25°C and 180 rpm for 24 hours. Subsequently, the total protein of *T. guizhouense* was extracted. Briefly, mycelia were ground in liquid nitrogen and suspended in 1 ml of extraction buffer [50 mM tris-HCl (pH 7.5), 100 mM NaCl, 5 mM EDTA, and 1% Triton X-100] supplemented with 10 μl of PA cocktail. The lysate was centrifuged at 13,200 rpm for 20 min at 4°C, and the supernatant was incubated with anti-GFP agarose. Proteins eluted from agarose or supernatant fractions were analyzed through Western blot using antibodies against GFP (Yeasen, China) and phosphorylated p44/42 (Cell Signaling Technology, USA). This was followed by incubation with HRP-conjugated secondary antibodies, specifically anti-rabbit immunoglobulin G (IgG)–HRP (Yeasen, China) and anti-mouse IgG-HRP (Yeasen, China). Detection was subsequently performed using enhanced chemiluminescence.

Ergosterol extraction and HPLC analysis

T. guizhouense and its mutants were cultured in 50 ml of PDB at 25°C and 180 rpm for 24 hours, and the mycelia were collected and freeze-dried. Subsequently, the dried mycelia (200 mg) were combined with 3 ml of KOH-methanol solution (6 g of KOH dissolved in 5 ml of methanol and diluted with ddH_2O to 10 ml) and then incubated at 70°C in a water bath for 2 hours. The extraction products were mixed with 3 ml of n-hexane, followed by centrifugation at 3000*g* for 5 min to isolate the supernatant. The supernatants were blown dry under nitrogen, followed by resuspension in 500 μl of ethanol. Quantitative analysis was conducted using high-performance liquid chromatography (HPLC: Agilent Technologies, USA). The collected samples were separated by HPLC on C18 column (2.1 mm by 150 mm, 3.5 μm) with a mobile phase consisting of 95% methanol and 5% water and detected at 283-nm ultraviolet.

Measurements of membrane integrity and stability

To detect the content of Evans, strains (1×10^5 spores) were cultured in PDB at 25°C and 180 rpm for 24 hours and then exposed to a 0.01% Evan's blue solution for 15 min, followed by three times for washing with 0.1 M $CaCl_2$ solution (pH 5.6). Subsequently, the mycelia were weighed and ground in liquid nitrogen. The supernatant was collected after adding 1% SDS for lysing for 20 min and centrifugation at 13,000*g* for 10 min. The optical density of the resulting supernatants was spectrophotometrically measured at 600 nm. The standard curve was generated using Evan's blue.

For PI staining, protoplasts from different strains were prepared by gradient centrifugation. Mycelia were placed into Solution A [$MgSO_4 \cdot 7H_2O$, 0.2 M Na_2HPO_4 and 0.2 M NaH_2PO_4, and 1.5% lyase (pH 5.5)] for 2 hours and then divided into a 15-ml tube. Solution B [0.6 M sorbitol and 1 M tris-HCl (pH 7.5)] was then added onto the top of solution A and centrifuged at 5000*g* for 15 min. A pipette was used to extract protoplasts from the middle layer. A total of 0.075% Triton CG-110 was added before staining with 10 μl of 1.5 mM PI solution. The samples were resuspended and analyzed using BD FACSCanto II Flow Cytometry (BD Biosciences, USA). A minimum

of 10,000 events were collected and excited by a 48-nm laser line after establishing exclusion gates based on forward scatter and side scatter to eliminate cellular debris.

To stain the germlings with Hoechst and PI, fresh conidia were incubated on the coverslip with 500 μl of PDB or PDB with 0.075% Triton CG-110 at 28°C for 16 hours. After incubation, germlings were washed with PBS and stained with Hoechst (10 μg/ml; Beyotime) for 5 min, followed by a wash with PBS. Subsequently, PI (5 μg/ml; Beyotime) was added, and then, the germlings were incubated for 5 min. After three washes with PBS, germlings were observed under a Leica SP8 confocal microscope using appropriate settings for Hoechst (excitation 405 nm, emission 346 to 460 nm) and PI (excitation, 535 nm; emission, 617 nm).

Y1H assays

To confirm the binding of STE12 to the promoters of *ergs*, Y1H assay was carried out. Y1H plasmids were created using the ClonExpress MultiS One Step Cloning Kit (Vazyme, China). The cDNA of *ste12* was cloned into the Bam HI–cleaved pHIS vector, and the upstream 1-kb promoters of *ergs* were cloned into the Eco RI–cleaved pGADT7 vector separately. Each pair of plasmids was cotransformed separately into *S. cerevisiae* Y187 following the one-step yeast transformation protocol.

Transformants were spotted on SD-Leu-Trp and SD-Leu-Trp-His with 60 mM 3AT. The plates were incubated at 30°C for 48 hours. Three independent experiments were performed to confirm the Y1H results.

Electrophoretic mobility shift assay

The STE12 expression plasmid synthesized by Sangon Biotech was transformed into *E. coli* (BL21) competent cells for protein expression. The *E. coli* strain was grown at 37°C and 180 rpm and induced with 0.1 mM IPTG at 16°C for 16 hours. The recombinant protein expressed in *E. coli* cells was subsequently applied to a Ni^{2+} affinity column (Ni-NTA Superflow, Thermo Fisher Scientific) and washed with five column volumes of binding buffer. Elution of the recombinant proteins was achieved using 8 ml of elution buffer containing 250 mM imidazole [20 mM Na_2HPO_4, 250 mM imidazole, and 300 mM NaCl (pH 8.0)]. The purified proteins were concentrated using an ultrafiltration centrifuge tube (Millipore) and stored at −80°C for subsequent analysis.

An electrophoretic mobility shift assay was conducted utilizing a Chemiluminescent EMSA Kit (Beyotime, Shanghai). Specifically, 0.5 μg of His::STE12 protein was combined with 1 μl of biotin-labeled probe (1 ng) and incubated at 25°C for 20 min. The sequences of these probes are provided in Supplementary Data.

Calculation of nitrogen use efficiency

The wild-type strain was inoculated onto PDA supplemented with 0.4 g of ^{15}N-labeled KNO_3 or it containing 0.075% Triton CG-110 at 25°C for 48 hours. Subsequently, the mycelium was collected and lyophilized. A 2 mg of dried mycelial powder was weighed for isotopic analysis using Delta V Advantage (Thermo Fisher Scientific, USA).

Supplementary Materials

The PDF file includes:
Figs. S1 to S9
Legends for tables S1 and S2

Other Supplementary Material for this manuscript includes the following:
Tables S1 and S2

REFERENCES AND NOTES

1. A. T. de Araújo-Ramos, M. T. Passoni, M. A. Romano, R. M. Romano, A. J. Martino-Andrade, Controversies on endocrine and reproductive effects of glyphosate and glyphosate-based herbicides: A mini-review. *Front. Endocrinol.* **12**, 627210 (2021).
2. L. Leino, T. Tall, M. Helander, I. Saloniemi, K. Saikkonen, S. Ruuskanen, P. Puigbo, Classification of the glyphosate target enzyme (5-enolpyruvylshikimate-3-phosphate synthase) for assessing sensitivity of organisms to the herbicide. *J. Hazard. Mater.* **408**, 124556 (2021).
3. M. B. Vazquez, M. V. Moreno, M. R. Amodeo, M. V. Bianchinotti, Effects of glyphosate on soil fungal communities: A field study. *Rev. Argent. Microbiol.* **4**, 349–358 (2021).
4. L. O. Correa, A. F. M. Bezerra, L. R. S. Honorato, A. C. A. Cortez, J. V. B. Souza, E. S. Souza, Amazonian soil fungi are efficient degraders of glyphosate herbicide; novel isolates of *Penicillium*, *Aspergillus*, and *Trichoderma*. *Braz. J. Biol.* **83**, e242830 (2023).
5. R. Mesnage, N. Oestreicher, F. Poirier, V. Nicolas, C. Boursier, C. Vélot, Transcriptome profiling of the fungus *Aspergillus nidulans* exposed to a commercial glyphosate-based herbicide under conditions of apparent herbicide tolerance. *Environ. Res.* **182**, 109116 (2020).
6. V. Nicolas, N. Oestreicher, C. Vélot, Multiple effects of a commercial Roundup® formulation on the soil filamentous fungus *Aspergillus nidulans* at low doses: Evidence of an unexpected impact on energetic metabolism. *Environ. Sci. Pollut. Res.* **23**, 14393–14404 (2016).
7. Z. Yu, R. Fischer, Light sensing and responses in fungi. *Nat. Rev. Microbiol.* **17**, 25–36 (2019).
8. Y. Li, Y. Li, H. Lu, T. Sun, J. Gao, J. Zhang, Q. Shen, Z. Yu, The bZIP transcription factor ATF1 regulates blue light and oxidative stress responses in *Trichoderma guizhouense*. *mLife* **2**, 365–377 (2023).
9. D. Frawley, M. C. Stroe, B. R. Oakley, T. Heinekamp, M. Strassburger, A. B. Fleming, A. A. Brakhage, O. Bayram, The pheromone module steC-MkkB-MpkB-SteD-HamE regulates development, stress responses and secondary metabolism in *Aspergillus fumigatus*. *Front. Microbiol.* **11**, 811 (2020).
10. D. Frawley, O. Bayram, The pheromone response module, a mitogen-activated protein kinase pathway implicated in the regulation of fungal development, secondary metabolism and pathogenicity. *Fungal Genet. Biol.* **144**, 103469 (2020).
11. D. Frawley, C. Greco, B. Oakley, M. M. Alhussain, A. B. Fleming, N. P. Keller, Ö. Bayram, The tetrameric pheromone module SteC-MkkB-MpkB-SteD regulates asexual sporulation, sclerotia formation and aflatoxin production in *Aspergillus flavus*. *Cell. Microbiol.* **22**, e13192 (2020).
12. Ö. Bayram, Ö. S. Bayram, Y. L. Ahmed, J.-i. Maruyama, O. Valerius, S. O. Rizzoli, R. Ficner, S. Irniger, G. H. Braus, The *Aspergillus nidulans* MAPK module AnSte11-Ste50-Ste7-Fus3 controls development and secondary metabolism. *PLOS Genet.* **8**, e1002816 (2012).
13. P. Alves de Castro, C. Figueiredo Pinzan, T. F. dos Reis, C. Valero, N. Van Rhijn, C. Menegatti, I. L. de Freitas Migliorini, M. Bromley, A. B. Fleming, A. M. Traynor, Ö. Sarikaya-Bayram, Ö. Bayram, I. Malavazi, F. Ebel, J. C. J. Barbosa, T. Fill, M. T. Pupo, G. H. Goldman, *Aspergillus fumigatus* mitogen-activated protein kinase MpkA is involved in gliotoxin production and self-protection. *Nat. Commun.* **15**, 33 (2024).
14. X. Hu, D. S. Hoffmann, M. Wang, L. Schuhmacher, M. C. Stroe, B. Schreckenberger, M. Elstner, R. Fischer, GprC of the nematode-trapping fungus *Arthrobotrys flagrans* activates mitochondria and reprograms fungal cells for nematode hunting. *Nat. Microbiol.* **9**, 1752–1763 (2024).
15. C.-Y. Kuo, R. J. Tay, H.-C. Lin, S.-C. Juan, G. Vidal-Diez de Ulzurrun, Y.-C. Chang, J. Hoki, F. C. Schroeder, Y.-P. Hsueh, The nematode-trapping fungus *Arthrobotrys oligospora* detects prey pheromones via G protein-coupled receptors. *Nat. Microbiol.* **9**, 1738–1751 (2024).
16. N. A. Brown, S. Schrevens, P. van Dijck, G. H. Goldman, Fungal G-protein-coupled receptors: Mediators of pathogenesis and targets for disease control. *Nat. Microbiol.* **3**, 402–414 (2018).
17. C. Jiang, X. Zhang, H. Liu, J. R. Xu, Mitogen-activated protein kinase signaling in plant pathogenic fungi. *PLOS Pathog.* **14**, e1006875 (2018).
18. J. Xie, J. M. Rybak, A. Martin-Vicente, X. Guruceaga, H. I. Thorn, A. V. Nywening, W. Ge, J. E. Parker, S. L. Kelly, P. D. Rogers, J. R. Fortwendel, The sterol C-24 methyltransferase encoding gene, *erg6*, is essential for viability of Aspergillus species. *Nat. Commun.* **15**, 4261 (2024).
19. Z. Liu, Y. Jian, Y. Chen, H. C. Kistler, P. He, Z. Ma, Y. Yin, A phosphorylated transcription factor regulates sterol biosynthesis in *Fusarium graminearum*. *Nat. Commun.* **10**, 1228 (2019).
20. T. Sun, Y. Li, J. Li, J. Gao, J. Zhang, R. Fischer, Q. Shen, Z. Yu, Red and far-red light improve the antagonistic ability of *Trichoderma guizhouense* against phytopathogenic fungi by promoting phytochrome-dependent aerial hyphal growth. *PLOS Genet.* **20**, e1011282 (2024).
21. S. L. Woo, R. Hermosa, M. Lorito, E. Monte, *Trichoderma*: A multipurpose, plant-beneficial microorganism for eco-sustainable agriculture. *Nat. Rev. Microbiol.* **21**, 312–326 (2023).

22. E. French, I. Kaplan, A. Iyer-Pascuzzi, C. H. Nakatsu, L. Enders, Emerging strategies for precision microbiome management in diverse agroecosystems. *Nat. Plants* **7**, 256–267 (2021).
23. A. Aramrak, K. K. Kidwell, C. M. Steber, I. C. Burke, Molecular and phylogenetic characterization of the homoeologous EPSP Synthase genes of allohexaploid wheat, Triticum aestivum (L.). *BMC Genomics* **16**, 844 (2015).
24. N. Defarge, E. Takács, V. L. Lozano, R. Mesnage, J. Spiroux de Vendômois, G.-E. Séralini, A. Székács, Co-formulants in glyphosate-based herbicides disrupt aromatase activity in human cells below toxic levels. *Int. J. Environ. Res. Public Health* **13**, 264 (2016).
25. L. Carretta, A. Cardinali, R. Masin, G. Zanin, H. Cederlund, Decyl glucoside surfactant Triton CG-110 does not significantly affect the environmental fate of glyphosate in the soil at environmentally relevant concentrations. *J. Hazard. Mater.* **388**, 122111 (2020).
26. R. Mesnage, C. Benbrook, M. N. Antoniou, Insight into the confusion over surfactant co-formulants in glyphosate-based herbicides. *Food Chem. Toxicol.* **128**, 137–145 (2019).
27. H. Zhan, Y. Feng, X. Fan, S. Chen, Recent advances in glyphosate biodegradation. *Appl. Microbiol. Biotechnol.* **102**, 5033–5043 (2018).
28. J.-W. Zhang, D.-Q. Xu, X.-Z. Feng, The toxic effects and possible mechanisms of glyphosate on mouse oocytes. *Chemosphere* **237**, 124435 (2019).
29. R. G. de Paula, A. C. C. Antoniêto, C. B. Carraro, D. C. B. Lopes, G. F. Persinoti, N. T. A. Peres, N. M. Martinez-Rossi, R. Silva-Rocha, R. N. Silva, The duality of the MAPK signaling pathway in the control of metabolic processes and cellulase production in *Trichoderma reesei*. *Sci. Rep.* **8**, 14931 (2018).
30. Y. Li, J. Zhang, Q. Shen, Z. Yu, Dual function of a fungal GPCR in activating mitochondrial respiration and initiating prey hunting in fungus-nematode interactions. *Innov. Life* **2**, 100087 (2024).
31. Y. Li, T. Sun, D. Guo, J. Gao, J. Zhang, F. Cai, R. Fischer, Q. Shen, Z. Yu, Comprehensive analysis of the regulatory network of blue-light-regulated conidiation and hydrophobin production in *Trichoderma guizhouense*. 23, 6241–6256 (2021).
32. J. Krüger, G. Loubradou, E. Regenfelder, A. Hartmann, R. Kahmann, Crosstalk between cAMP and pheromone signalling pathways in *Ustilago maydis*. *Mol. Gen. Genet.* **260**, 193–198 (1998).
33. D. Lanver, A. Mendoza-Mendoza, A. Brachmann, R. Kahmann, Sho1 and Msb2-related proteins regulate appressorium development in the smut fungus *Ustilago maydis*. *Plant Cell* **22**, 2085–2101 (2010).
34. E. Pérez-Nadales, A. Di Pietro, The membrane mucin Msb2 regulates invasive growth and plant infection in *Fusarium oxysporum*. *Plant Cell* **23**, 1171–1185 (2011).
35. W. Liu, X. Zhou, G. Li, L. Li, L. Kong, C. Wang, H. Zhang, J.-R. Xu, Multiple plant surface signals are sensed by different mechanisms in the rice blast fungus for appressorium formation. *PLOS Pathog.* **7**, e1001261 (2011).
36. M. Osés-Ruiz, N. Cruz-Mireles, M. Martin-Urdiroz, D. M. Soanes, A. B. Eseola, B. Tang, P. Derbyshire, M. Nielsen, J. Cheema, V. Were, I. Eisermann, M. J. Kershaw, X. Yan, G. Valdovinos-Ponce, C. Molinari, G. R. Littlejohn, B. Valent, F. L. H. Menke, N. J. Talbot, Appressorium-mediated plant infection by *Magnaporthe oryzae* is regulated by a Pmk1-dependent hierarchical transcriptional network. *Nat. Microbiol.* **6**, 1383–1397 (2021).
37. Z. Guo, X. Liu, N. Wang, P. Mo, J. Shen, M. Liu, H. Zhang, P. Wang, Z. Zhang, Membrane component ergosterol builds a platform for promoting effector secretion and virulence in *Magnaporthe oryzae*. *New Phytol.* **237**, 930–943 (2023).
38. K. Tanaka, K. Tatebayashi, A. Nishimura, K. Yamamoto, H.-Y. Yang, H. Saito, Yeast Osmosensors Hkr1 and Msb2 activate the Hog1 MAPK cascade by different mechanisms. *Sci. Signal.* **7**, ra21 (2014).
39. N. Vadaie, H. Dionne, D. S. Akajagbor, S. R. Nickerson, D. J. Krysan, P. J. Cullen, Cleavage of the signaling mucin Msb2 by the aspartyl protease Yps1 is required for MAPK activation in yeast. *J. Cell Biol.* **181**, 1073–1081 (2008).
40. N. Sajjad, E. A. Bhat, D. Shah, I. Manzoor, W. Noor, S. Shah, S. Hassan, R. Ali, 12 - Nitrogen uptake, assimilation, and mobilization in plants under abiotic stress, in *Transporters and Plant Osmotic Stress*, A. Roychoudhury, D. K. Tripathi, R. Deshmukh, Eds. (Academic Press, 2021).
41. A. P. MacCabe, S. Vanhanen, M. D. Sollewijn Gelpke, P. J. I. van de Vondervoort, H. N. Arst, J. Visser, Identification, cloning and sequence1 of the *Aspergillus niger areA* wide domain regulatory gene controlling nitrogen utilisation. *Biochim. Biophys. Acta* **1396**, 163–168 (1998).
42. R. Ruan, Y. Chen, H. Li, M. Wang, Functional diversification of sterol regulatory element binding proteins following gene duplication in a fungal species. *Fungal Genet. Biol.* **131**, 103239 (2019).
43. L. Tan, L. Chen, H. Yang, B. Jin, G. Kim, Y. J. Im, Structural basis for activation of fungal sterol receptor Upc2 and azole resistance. *Nat. Chem. Biol.* **18**, 1253–1262 (2022).
44. Y.-L. O. Yuan, S. Fields, Properties of the DNA-binding domain of the *Saccharomyces cerevisiae* STE12 Protein. *Mol. Cell. Biol.* **11**, 5910–5918 (1991).

Acknowledgments

Funding: This work was supported by the National Key R&D Program of China (grant no. 2024YFD1700701 to Z.Y.), the National Natural Science Foundation of China (NSFC) (grant nos. 32270053 and 32070101) (to Z.Y.), the Science Fund for Distinguished Young Scholars of Jiangsu Province (grant no. BK20240091) (to Z.Y.), the Natural Science Foundation of Jiangsu Province (grant no. BK20241554) (to Y.L.), the China Postdoctoral Science Foundation (grant no. 2024M751441) (to Y.L.), the Fundamental Research Funds for the Central Universities (grant no. KYT2024001) (to Z.Y.), the Outstanding Postdoctoral Program of Jiangsu Province (grant no. 2024ZB328) (to Y.L.), and the Postdoctoral Fellowship Program of CPSF (grant no. GZC20240711) (Y.L.). **Author contributions:** Conceptualization: Z.Y., Q.S., J.G., Y.L., X.L., and J.P. Methodology: J.P., X.L., Z.Y., and J.Z. Investigation: Z.Y., P.J., and X.L. Resources: Q.S., J.Z., J.P., and Z.Y. Funding acquisition: Z.Y. and Y.L. Data curation: X.L., and Z.Y. Visualization: J.P., and Z.Y. Validation: X.L., and J.P. Formal analysis: X.L. and J.P. Writing—original draft: J.P., X.L., and Z.Y. Writing—review and editing: F.Q. and Z.Y. Supervision: Z.Y. Project administration: Z.Y.
Competing interests: The authors declare that they have no competing interests.
Data and materials availability: All data needed to evaluate the conclusions in the paper are present in the paper and/or the Supplementary Materials.

Submitted 20 October 2024
Accepted 24 January 2025
Published 28 February 2025
10.1126/sciadv.adt8715